Maximizing product concentration in a diabatic multistage reactor

M. M. Saleh[1] M. I. Nelson[2]

(Received 22 December 2015; revised 18 July 2016)

Abstract

We develop a mathematical model describing the operation of autothermal processes. Autothermal reactors provide considerable thermal efficiency over conventional reactors. The reaction mechanism investigated is $A \to B \to C$, where the reactions occur in a two reactor cascade. Specific features of coupled endothermic and exothermic reactions are taken into account. Particular considerations are presented and discussed for different catalysts to obtain 90% conversion into product.

http://journal.austms.org.au/ojs/index.php/ANZIAMJ/article/view/10387 gives this article, © Austral. Mathematical Soc. 2016. Published August 1, 2016, as part of the Proceedings of the 12th Biennial Engineering Mathematics and Applications Conference. ISSN 1446-8735. (Print two pages per sheet of paper.) Copies of this article must not be made otherwise available on the internet; instead link directly to this URL for this article.

Contents

1 Introduction

Autothermal processes are important when exothermic reactions, in which the system releases heat, are coupled with endothermic reactions, in which the system absorbs heat. In conventional reactors, energy must be supplied

for endothermic reactions to proceed. This is typically supplied by external burners or interstage heaters. In autothermal reactors the required heat is supplied by exothermic reactions. If the autothermal system is correctly set up, then the overall reaction process is energy neutral. Autothermal reactors are an attractive solution in the implementation of high temperature reactors for reactions with overall exothermicity because of their high thermal efficiency. The absence of an external burner and the accompanying power supply makes an autothermal process both simpler and less expensive. A promising application of autothermal processes is in improving the operating conditions by minimizing heat consumption [6]. In particular, autothermal reactors have potential applications in the steam reforming of light alkanes for hydrogen generation in on-board vehicular fuel cells or in the production of syngas, a gaseous fuel that is a mixture of hydrogen, carbon monoxide and often carbon dioxide [8]. Autothermal reactors are efficient in the production of H_2 from steam reforming of methanol [9] and in optimising oxidation and steam reforming for methane conversion [11].

The world is currently facing critical challenges in terms of meeting future energy requirements while reducing green house emissions. With rising oil prices and a possible 'peak' in oil resources, the conversion of natural gas into syngas for production of liquid fuels and/or hydrogen will become crucial for the economy and standard of living. Our aim is to develop a mathematical model which describes the operation of autothermal processes to maximize the product concentration.

2 Chemistry of the model

We consider a chemical reaction in which a reactant A is converted to a product C. The reaction mechanism consists of two steps. In the first step the reactant A is converted into an intermediate B. In the second step the

Figure 1: Prototype reactor configuration, where A_0 is the feed concentration, T_0 is the feed temperature, and q is the flow rate.

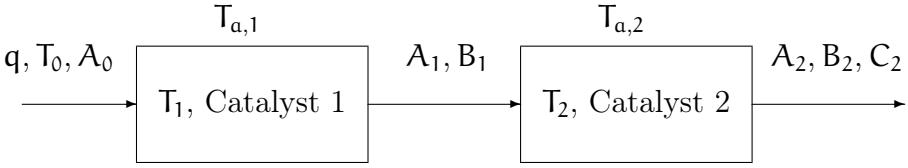

intermediate B is converted into the final product C:

$$A \rightarrow B, \tag{1}$$
$$B \rightarrow C. \tag{2}$$

We assume that the first reaction is endothermic, that is, heat is required to drive the reaction, whereas the second reaction is exothermic, that is, heat is produced by the reaction. The reaction is assumed to take place in a two reactor cascade. The catalyst for reaction (1) is placed in reactor one whilst the catalyst for reaction (2) is placed in reactor two. Consequently, the first (second) reaction only occurs in the first (second) reactor.

Figure 1 shows the processes that occur in the reactor cascade. The concentrations of the reactant A and the intermediate B leaving reactor one are A_1 and B_1, respectively. The concentrations of the reactant A and the intermediate B and the product C leaving reactor two are A_2, B_2 and C_2, respectively. The coolant temperatures for the two reactors are $T_{a,1}$ and $T_{a,2}$, respectively. The temperatures of the reacting mixtures in reactor one and two are T_1 and T_2, respectively.

We are particularly interested in identifying catalysts and reactor operation conditions that ensure a minimum of 90% conversion of reactant A to product C.

3 Model equations

In Section 3.1 we introduce the assumption for the reaction schemes (1) and (2). In Section 3.2 we give the model equations for the reaction schemes (1) and (2). In Section 3.3 we non-dimensionalise the model.

Gray and Scott [5, Chap. 7] overviewed the model equations for the classic chemical engineering problem of a non-isothermal continuously stirred tank reactor. Recall that our reactor configuration consists of a cascade of two reactors. The effluent stream from reactor one provides the feed stream for reactor two. Consequently, our model equations are obtained by straighforwardly adapting the model for a single reactor. Dangelmayr and Stewart [2] studied the model equations for a similar system, in which an exothermic reaction occurs in both reactors.

3.1 Model assumptions

It is assumed that the reactor vessels are well stirred. We consider a feed temperature to be realistic if $T_0 \leqslant 1000\,\mathrm{K}$. It is often useful to characterise a chemical reaction in terms of a 'characteristic temperature' [10]. We write the pre-exponential factor a_i in terms of a characteristic temperature T_{ci} [10]:

$$a_i = \frac{E_i \alpha}{R T_{ci}^2} \exp\left[\frac{E_i}{R T_{ci}}\right],$$

for reactor $i = 1, 2$, where E_i is the activation energy, R is the ideal gas constant, and α is a constant heating rate.

The residence time in both reactor is defined by

$$\tau_i = \frac{V_i}{q},$$

for $i = 1, 2$, where V_i is the reactor volume and q is the flow-rate.

3.2 Dimensional equations

The system of equations in the first reactor are

$$V_1 \frac{dA_1}{dt} = q(A_0 - A_1) - V_1 a_1 \exp\left[\frac{-E_1}{RT_1}\right] A_1 \,, \tag{3}$$

$$V_1 \frac{dB_1}{dt} = -qB_1 + V_1 a_1 \exp\left[\frac{-E_1}{RT_1}\right] A_1 \,, \tag{4}$$

$$V_1 \frac{dC_1}{dt} = -qC_1 \,, \tag{5}$$

$$c_{pg}\rho_g V_1 \frac{dT_1}{dt} = qc_{pg}\rho_g(T_0 - T_1) - Q_1 V_1 a_1 \exp\left[\frac{-E_1}{RT_1}\right] A_1 - J_1 \chi_1 S_1 (T_1 - T_{a,1}) \,. \tag{6}$$

The system of equations in the second reactor are

$$V_2 \frac{dA_2}{dt} = q(A_1 - A_2) \,, \tag{7}$$

$$V_2 \frac{dB_2}{dt} = q(B_1 - B_2) - V_2 a_2 \exp\left[\frac{-E_2}{RT_2}\right] B_2 \,, \tag{8}$$

$$V_2 \frac{dC_2}{dt} = q(C_1 - C_2) + V_2 a_2 \exp\left[\frac{-E_2}{RT_2}\right] B_2 \,, \tag{9}$$

$$c_{pg}\rho_g V_2 \frac{dT_2}{dt} = qc_{pg}\rho_g(T_1 - T_2) + Q_2 V_2 a_2 \exp\left[\frac{-E_2}{RT_2}\right] B_2 - J_2 \chi_2 S_2 (T_2 - T_{a,2}) \,. \tag{10}$$

The nomenclature is defined in Table 1.

The concentrations flowing into reactor two are the concentrations exiting from reactor one. Similarly, the temperature of the fluid entering reactor two is equal to that leaving reactor one.

We are interested in the *long-time* behaviour of the reactor cascade. The system of eight equations, (3)–(10), can be reduced to a system of five

Table 1: Definitions and units of terms that appear in the model equations (3)–(10). The index i takes values 1 or 2, referring to a property in either reactor one or reactor two.

parameter	definition
A_i, B_i, C_i ($\mathrm{mol\,m^{-3}}$)	concentrations of reactant A, intermediate B and product C
A_0 ($\mathrm{mol\,m^{-3}}$)	concentration of reactant A in the feed
T_i (K)	temperature inside the reactors
T_0 (K)	feed temperature
$T_{a,i}$ (K)	temperature of the reactor walls
E_i ($\mathrm{J\,mol^{-1}}$)	activation energy
Q_i ($\mathrm{J\,mol^{-1}}$)	modulus of a heat of reaction
S_i ($\mathrm{m^2}$)	internal surface area
V_i ($\mathrm{m^3}$)	reactor volume
R ($\mathrm{J\,K^{-1}mol^{-1}}$)	ideal gas constant
a_i ($\mathrm{s^{-1}}$)	pre-exponential factor
J_i	a constant, $J_i = 0$ in the adiabatic case and $J_i = 1$ in the diabatic case
q ($\mathrm{m^3 s^{-1}}$)	flow-rate
t (s)	time
χ_i ($\mathrm{J\,s^{-1}m^{-2}K^{-1}}$)	heat transfer coefficient between the reaction mixture and the reactor walls
c_{p_g} ($\mathrm{J\,K^{-1}kg^{-1}}$)	heat capacity of the reaction mixture
ρ_g ($\mathrm{kg\,m^{-3}}$)	density of the reaction mixture

equations—equations for B_1, C_1 and C_2 are not required. As we are interested in the *long-time* behaviour we study only the steady-state solutions and determine their behavior.

3.3 Dimensionless equations

The reduced system of non-dimensional equations in the first reactor obtained from equations (3)–(6) is

$$\frac{dA_1^*}{dt^*} = \frac{1 - A_1^*}{\tau_1^*} - a_1^* \exp\left[\frac{-E_1^*}{\theta_1}\right] A_1^* , \tag{11}$$

$$\frac{d\theta_1}{dt^*} = \frac{\theta_0 - \theta_1}{\tau_1^*} - Q_1^* a_1^* \exp\left[\frac{-E_1^*}{\theta_1}\right] A_1^* - J_1 \chi_{T,1}^* (\theta_1 - \theta_{a,1}) , \tag{12}$$

$$B_1^*(t^*) = 1 - A_1^*(t^*) , \tag{13}$$

$$C_1^*(t^*) = 0 . \tag{14}$$

The reduced system of non-dimensional equations in the second reactor obtained from equations (7)–(10) is

$$\frac{dA_2^*}{dt^*} = \frac{A_1^* - A_2^*}{\tau_2^*} , \tag{15}$$

$$\frac{dB_2^*}{dt^*} = \frac{1 - A_1^* - B_2^*}{\tau_2^*} - a_2^* \exp\left[\frac{-1}{\theta_2}\right] B_2^* , \tag{16}$$

$$\frac{d\theta_2}{dt^*} = \frac{\theta_1 - \theta_2}{\tau_2^*} + Q_2^* a_2^* \exp\left[\frac{-1}{\theta_2}\right] B_2^* - J_2 (\theta_2 - \theta_{a,2}) , \tag{17}$$

$$C_2^* = 1 - A_2^* - B_2^* . \tag{18}$$

In the above equations we use the dimensionless concentrations $A_i^* = A_i / A_0$, $B_i^* = B_i / A_0$, $C_i^* = C_i / A_0$, dimensionless temperatures $\theta_i = (RT_i)/E_2$ where $i = 1, 2$, and dimensionless time $t^* = (\chi_2 S_2 t)/(c_{p_g} \rho_g V_2)$.

The dimensionless parameters are: the temperature in the feed $\theta_0 = (RT_0)/E_2$; the temperature of reactor walls $\theta_{a,i} = (RT_{a,i})/E_2$; the activation energy

in reactor one $E_1^* = E_1/E_2$; the modulus of a heat of reaction $Q_i^* = (A_0 R Q_i)/(E_2 c_{p_g} \rho_g)$; the characteristic temperature $T_{ci}^* = (RT_{ci})/E_2$; the volume $V^* = V_1/V_2$; the residence time $\tau_i^* = (\chi_2 S_2 \tau_i)/(c_{p_g} \rho_g V_2)$; the heat-transfer rate in reactor one $\chi_{T,1}^* = (\chi_1 S_1 V_2)/(\chi_2 S_2 V_1)$; the heating rate constant $\alpha^* = (\alpha \rho_g c_{pg} R V_2)/(\chi_2 E_2 S_2)$; the pre-exponential factor in reactor two $a_2^* = (\alpha^*/T_{c2}^{*2}) \exp[1/T_{c2}^*]$; and the pre-exponential factor in reactor one

$$a_1^* = \frac{\alpha^* V^* E_1^*}{T_{c1}^{*2}} \exp\left[\frac{E_1^*}{T_{c1}^*}\right]. \tag{19}$$

4 Results and Discussion

All calculations performed in this article use the the parameter values stated in Appendix A, unless otherwise stated.

4.1 Achieving 90% conversion in reactor one

To achieve 90% conversion of the reactant A into the product C we must achieve at least 90% conversion of the reactant into the intermediate species B in the first reactor. By taking a suitable linear combination of equations (11) and (12) we find an equation giving the feed temperature required to achieve a specified steady-state value of the reactant concentration:

$$\theta_0 = \frac{-(1 + J_1 \tau_1^* \chi_1^*) E_1^*}{\log[(1 - A_1^*)/(a_1^* A_1^* \tau_1^*)]} + Q_1^*(1 - A_1^*) - J_1 \tau_1^* \chi_1^* \theta_{a,1}\,. \tag{20}$$

Recall from equation (19) that the pre-exponential factor a_1^* depends on the activation energy E_1^*. Differentiating (20) with respect to the activation energy E_1^* we obtain

$$\frac{d\theta_0}{dE_1^*} = -(1 + J_1 \tau_1^* \chi_1^*) \left(\frac{E_1^* + T_{c1}^* + T_{c1}^* \log[(1 - A_1^*)/(a_1^* A_1^* \tau_1^*)]}{T_{c1}^* (\log[(1 - A_1^*)/(a_1^* A_1^* \tau_1^*)])^2} \right) < 0\,, \tag{21}$$

Table 2: The inflow temperature T_0 (K) required to achieve 90% conversion in the first reactor $A_1^* = 0.1$ as a function of the activation energy E_1 (kJ mol^{-1}) and the characteristic temperature T_{c1} (K). The heat of endothermicity is $Q_1 = 205.8$ kJ mol^{-1} and the coolant temperature is $T_{a,1} = 800$ K.

T_{c1}	$T_0\,(E_1 = 50)$	$T_0\,(E_1 = 80)$	$T_0\,(E_1 = 120)$	$T_0\,(E_1 = 180)$
342	1021.9	964.6	940.6	927.4
442	1258.6	1126.2	1076.1	1049.5
542	1602.7	1319.8	1226.5	1179.4

for $\tau_1^* < [(1 - A_1^*)/(a_1^* A_1^*)] \exp[1 + (E_1^*/T_{c1}^*)]$ (this holds for our parameter values in Appendix A).

Equation (21) shows that the required inflow temperature is a decreasing function of E_1^*, that is, a lower activation energy requires a higher inflow temperature to achieve a specified conversion.

Differentiating (20) with respect to the characteristic temperature T_{c1}^*, and using equation (19), we obtain

$$\frac{d\theta_0}{dT_{c1}^*} = \frac{E_1^*(1 + J_1\tau_1^*\chi_1^*)(2T_{c1}^* + E_1^*)}{T_{c1}^{*2}\{\log[(1 - A_1^*)/(a_1^* A_1^* \tau_1^*)]\}^2} > 0\,. \tag{22}$$

Equation (22) shows that the required inflow temperature is an increasing function of T_{c1}, that is, a higher characteristic temperature requires a higher inflow temperature to achieve a specified conversion.

Equations (21) and (22) show that the ideal catalyst for reactor one has a high activation energy E_1 and a low characteristic temperature T_{c1}. Returning to dimensional values, Table 2 shows feed temperatures T_0 that obtain a conversion of 90% of the reactant A_1 as a function of the catalyst parameters E_1 and T_{c1}. This table shows that for a high value of the endothermicity Q_1, the required feed temperature T_0 is almost always unrealistic, that is, higher than 1000 K.

Figure 2: The parameter values required to achieve 90% conversion in the first reactor as a function of the activation energy E_1 and the characteristic temperature T_{c1}. The feed temperature $T_0 = 1000\,\mathrm{K}$ and the coolant temperature $T_{a,1} = 800\,\mathrm{K}$. The heat of endothermicity Q_1 is (a) $50\ \mathrm{kJ\,mol^{-1}}$, (b) $100\ \mathrm{kJ\,mol^{-1}}$, (c) $150\ \mathrm{kJ\,mol^{-1}}$ and (d) $205.8\ \mathrm{kJ\,mol^{-1}}$. All other parameters values are given in Appendix A.

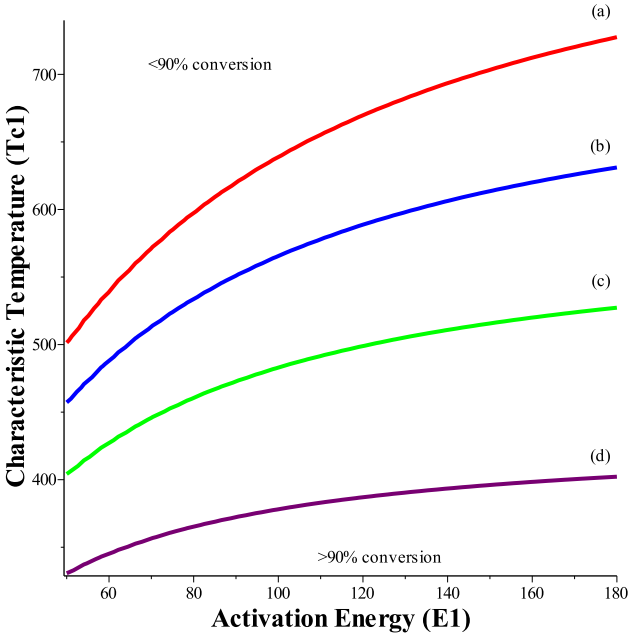

Figure 2 shows the parameter values required to achieve 90% conversion of the reactant A as a function of the heat of the activation energy E_1 and the characteristic temperature T_{c1} when the inflow temperature T_0 is fixed to its maximum value ($1000\,\mathrm{K}$) for different values of the heat of endothermicity Q_1. This figure confirms that there is a small range of parameter values for which 90% conversion is achieved for highly endothermic reactions.

Differentiating (20) with respect to the endothermicity parameter Q_1^* we

obtain

$$\frac{d\theta_0}{dQ_1^*} = -A_1^* + 1 > 0\,, \tag{23}$$

as $0 < A_1^* < 1$. Equation (23) shows that the required feed temperature is an increasing function of Q_1^*, that is, more endothermic reactions require a higher feed temperature to achieve a specified conversion, as shown in Figure 3. This figure show the inflow temperature required to achieve 90% conversion of the reactant A_1 in the first reactor as a function of the activation energy E_1, for different values of the characteristic temperature T_{c1} and the heat of endothermicity Q_1. Feed temperatures higher than 1000 K are considered to be unachievable inside these reactors. Figure 3 confirms that it is more difficult to find a suitable catalyst for more highly endothermic reactions. When the reaction is weakly endothermic there is a larger range of suitable catalysts.

Differentiating (20) with respect to the coolant temperature $\theta_{a,1}$ we obtain

$$\frac{d\theta_0}{d\theta_{a,1}} = -J_1\tau_1^*\chi_1^* < 0\,. \tag{24}$$

Equation (24) shows that the required inflow temperature is a decreasing function of $\theta_{a,1}$, that is, a higher coolant temperature requires a lower inflow temperature to achieve a specified conversion. Figure 4 shows that feed temperature T_0 is always realistic for any value of the coolant temperature $T_{a,1}$.

In conclusion, in order to achieve 90% conversion in the first reactor at a realistic feed temperature $T_0 < 1000$ K, the characteristic temperature T_{c1} and the heat of endothermicity Q_1 are required to be small, whereas the activation energy E_1 is required to be large. Finally, increasing the coolant temperature decreases the required value for the feed temperature.

Figure 3: The feed temperature T_0 required to achieve 90% conversion in the first reactor as a function of the activation energy E_1 for (top) $Q_1 = 205.8\,\mathrm{kJ\,mol^{-1}}$ and (bottom) $Q_1 = 50\,\mathrm{kJ\,mol^{-1}}$. The coolant temperature is $T_{a,1} = 800\,\mathrm{K}$ and the activation energy is $E_2 = 50\ \mathrm{kJ\,mol^{-1}}$. The dashed lines show the maximum value of the feed temperature. All other parameters are given in Appendix A.

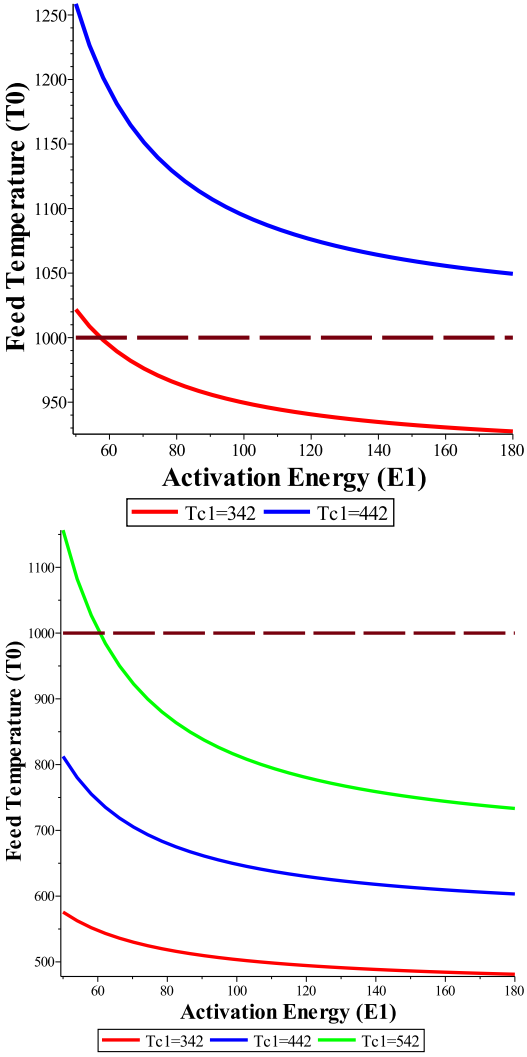

Figure 4: The feed temperature T_0 required to achieve 90% conversion in the first reactor as a function of the coolant temperature $T_{a,1}$. The characteristic temperature $T_{c1} = 342\,K$, the activation energy $E_1 = 80\ kJ\,mol^{-1}$ and the activation energy $E_2 = 50\ kJ\,mol^{-1}$. The heat of endothermicity Q_1 is (a) $50\ kJ\,mol^{-1}$, (b) $100\ kJ\,mol^{-1}$, (c) $150\ kJ\,mol^{-1}$ and (d) $205.8\ kJ\,mol^{-1}$. All other parameters are given in Appendix A.

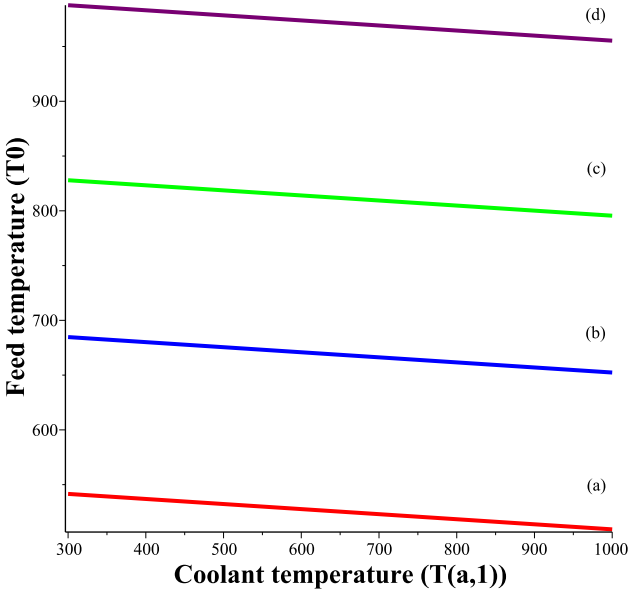

4.2 Achieving 90% conversion in reactor two

In this section we fix the catalyst in the first reactor to ensure slightly more than 90% conversion of the reactant A_1^*. We investigate how the choice of the catalyst in the second reactor effects the steady-state concentration C_2^*. We consider the case $E_2 = 50\,kJ\,mol^{-1}$ and $Q_2 = 100\,kJ\,mol^{-1}$ and examine different values for the characteristic temperature T_{c2}. Figures 5(a) and 5(b) are steady-state diagrams with red and black lines indicating stable and unstable states, respectively. The high branch is called the high conversion

Figure 5: The steady-state structure in the diabatic reactor when $Q_1 = 100\,\mathrm{kJ\,mol^{-1}}$, $Q_2 = 100\,\mathrm{kJ\,mol^{-1}}$, $E_1 = 80\,\mathrm{kJ\,mol^{-1}}$, $E_2 = 50\,\mathrm{kJ\,mol^{-1}}$, $T_{c1} = 342$ K, $T_0 = 680$ K, $T_{a,1} = 800$ K and: (a) $T_{c2} = 405$ K; and (b) $T_{c2} = 435$ K. All other parameters are given in Appendix A.

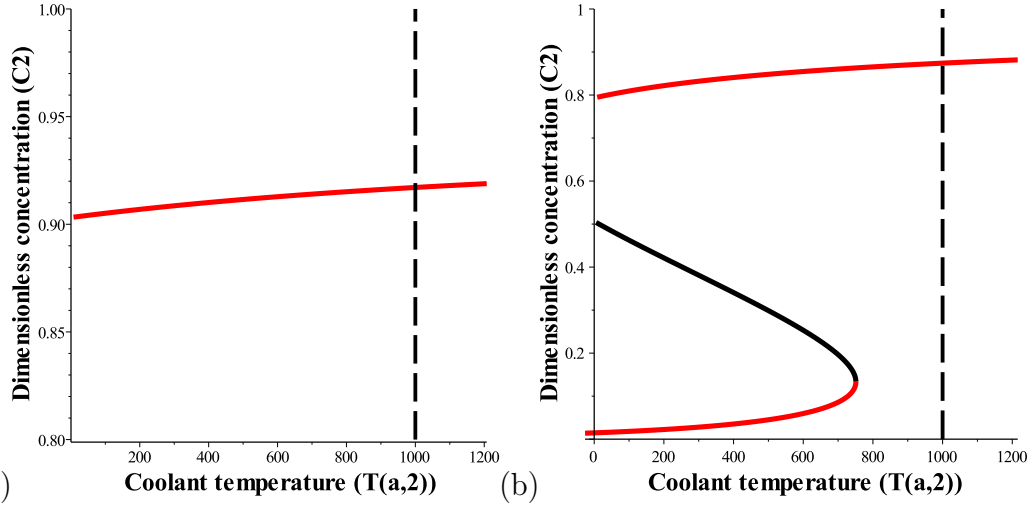

branch and the low branch is called the low conversion branch (both branches are red).

The steady-state diagrams shown in Figures 5(a)–(b) and 6(a)–(c) exhibit bistability, that is, there are parameter regions over which there are multiple stable steady-state solutions. Bistability is a common phenomenon in open chemically reacting systems with non-linear kinetics [5, 4]. In systems featuring exothermic reactions, bistability typically comprises stable steady-state solutions with 'low' and 'high' values.

In simplified systems the phenomena of bistability is easily demonstrated by plotting 'heat loss' and 'heat-generation' on the same figure [5, Fig. 7.2]. The essence of the situation is that whilst heat-loss is a linear function of the reactor temperature, heat-generation is a sigmoidal function of reactor temperature, thus the presence of bistability is a consequence of the non-

Figure 6: The steady-state structure in the diabatic reactor with the same parameters as Figure 5, except: (a) $T_{c2} = 442$ K; (b) $T_{c2} = 448$ K; (c) $T_{c2} = 464$ K; and (d) $T_{c2} = 511$ K. All other parameters are given in Appendix A.

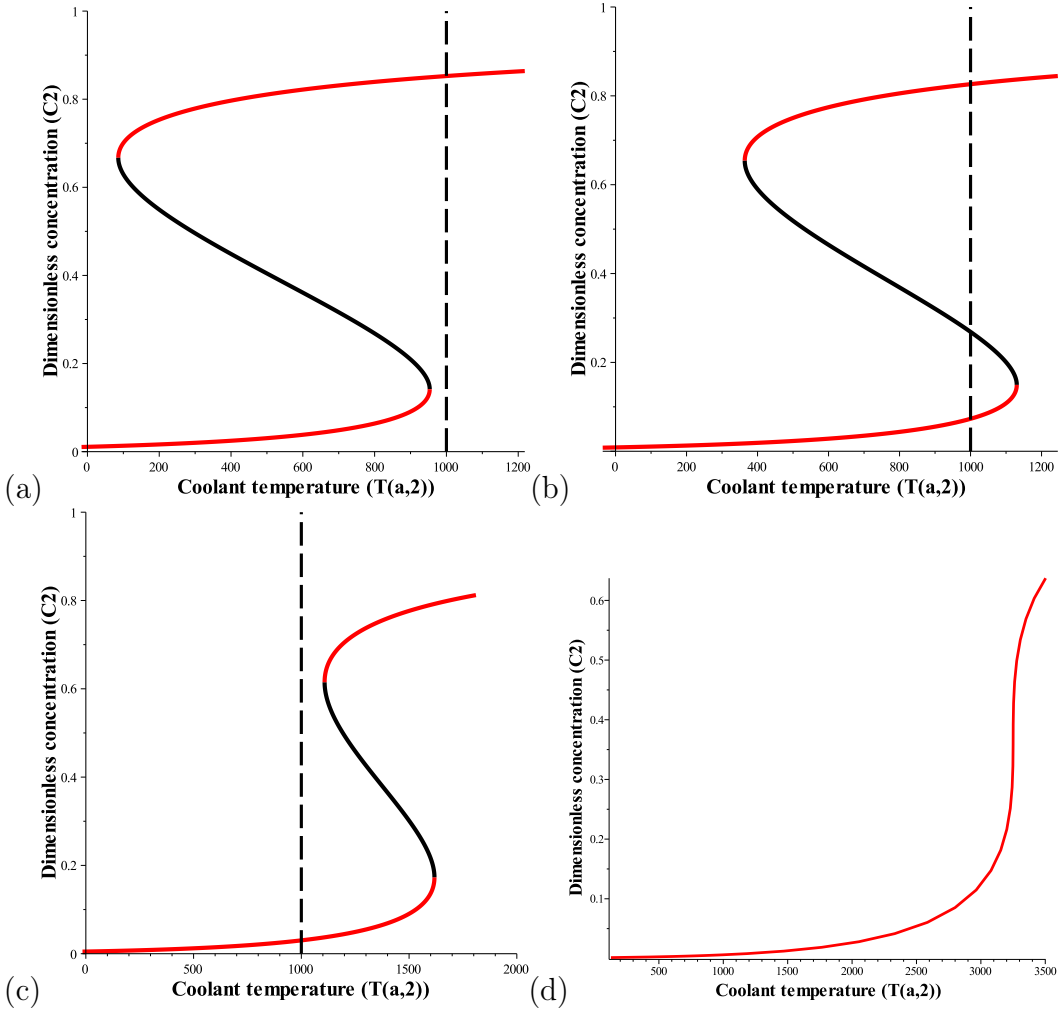

linearity of the heat-generation curve. Depending upon parameter values there are generically either one or three intersection points of the heat-loss and heat-generation plots. Bilous and Amundson [1, Fig. 2] pioneered the procedure of separating heat-loss and heat-generation and plotting them as functions of the reactor temperature.

4.2.1 Scenario one $T_{c1} < 408\,K$

Figure 5(a) shows the steady-state concentration diagram when $T_{c2} = 405\,K$. In this figure only positive values for the coolant temperature are shown as negative values are unnphysical. Thus the low conversion branch and the limit points are not shown as they occur on the negative axis.

In Figure 5(a) both the extinction and the ignition limit point bifurcations occur at unphysical values (negative!) of the coolant temperature $T_{a,2}$. The practical consequence of this is that the system always evolves to the high conversion branch. Consequently, this steady-state diagram is the best possible case as there is at least 90% conversion for all values of the coolant temperature of reactor two; a high coolant temperature is not required to ensure high product concentration. We consider the reaction in scenario one to be autothermal because it does not require heat to be supplied in order to obtain high conversion.

4.2.2 Scenario two $408\,K \leqslant T_{c1} < 441\,K$

The value of the characteristic temperature is increased to $T_{c2} = 435\,K$. The steady-state diagram is shown in Figure 5(b). The branches are disjoint as the extinction limit point occurs for a negative value of the coolant temperature. The value of the coolant temperature at the ignition limit point is now positive. High conversion can be achieved by temporarily increasing the value of the coolant temperature past that of the ignition limit point. It is then possible to decrease the coolant temperature to a lower value, in theory any other

value. This case is good in practice, provided that the coolant temperature at the ignition limit point is not too high. If the critical value of the coolant temperature is lower than 298 K, then in practice this case is indistinguishable from the first scenario.

4.2.3 Scenario three $441\,\mathrm{K} \leqslant T_{c1} < 444\,\mathrm{K}$

As the value of the characteristic temperature is further increased the next transition occurs when the value of the coolant temperature at the extinction limit point moves into the right half plane. The steady-state diagram following this transition is shown in Figure 6(a). As in the previous scenario the system can be moved to the high conversion branch by increasing the coolant temperature. However, there is now a minimum value of the coolant temperature that is required in order to operate on the high conversion branch. If the coolant temperature is decreased through this value, then the system will 'fall off' onto the low conversion branch. This case is good in practice, provided that the values of the coolant temperature at the extinction and ignition limit points are not too high.

4.2.4 Scenario four $444\,\mathrm{K} \leqslant T_{c1} < 462\,\mathrm{K}$

The next transition to occur is when the value of the coolant temperature at the ignition limit point moves through the maximum value of the coolant temperature $T_{a,2} = 1000\,\mathrm{K}$. Figure 6(b) is a steady-state diagram for this case. It is no longer possible to reach the high conversion branch by increasing the coolant temperature. Instead, a temporary perturbation of some kind must be imposed onto the system to 'kick' it from the low conversion branch onto the high conversion branch.

4.2.5 Scenario five $462\,\mathrm{K} \leqslant T_{c1} < 511\,\mathrm{K}$

Figure 6(c) shows the steady-state when both the ignition and extinction limit points have moved through the maximum value of the coolant temperature. It is now impossible to reach the high product conversion branch by either increasing the coolant temperature or by imposing a 'kick'. From a practical perspective, catalysts falling into this category are of no interest.

4.2.6 Scenario six $T_{c1} \geqslant 511\,\mathrm{K}$

The final transition to occur is a cusp singularity, at which the two limit points disappear. Figure 6(d) shows the steady-state diagram. For realistic values of the coolant temperature only a low conversion is achieved.

4.3 Limit point unfolding diagram

In Section 4.2 we discussed how the steady-state diagram changes as the characteristic temperature of the catalyst in the second reactor is increased. Figure 7 shows an unfolding limit point diagram. The red branches are the ignition (Lp) and extension (Ep) branches. The horizontal lines demonstrate different transitions between steady-state diagrams. For example, the line at $T_{c1} = 441\,\mathrm{K}$ separates the steady-state diagram 5(b) from the steady-state diagram 6(a). The values of the characteristic temperature at all the transitions described earlier are identified in Figure 7. This shows that we can determine the location of all the transitions from one figure.

5 Conclusions

We considered a kinetic model consisting of two sequential reactions, the first being endothermic whilst the second being exothermic. It is assumed

Figure 7: The unfolding diagram of the characteristic temperature for the case $E_2 = 50\ \mathrm{kJ\,mol^{-1}}$, $Q_2 = 100\ \mathrm{kJ\,mol^{-1}}$, $Q_1 = 100\ \mathrm{kJ\,mol^{-1}}$, $E_1 = 80\ \mathrm{kJ\,mol^{-1}}$, $T_{c1} = 342$ K, $T_0 = 680$ K and $T_{a,1} = 800$ K. All other parameters are given in Appendix A. The labels (a)–(f) relate to the steady-state diagrams shown in Figures 5(a)–(b) and 6(a)–(d), respectively.

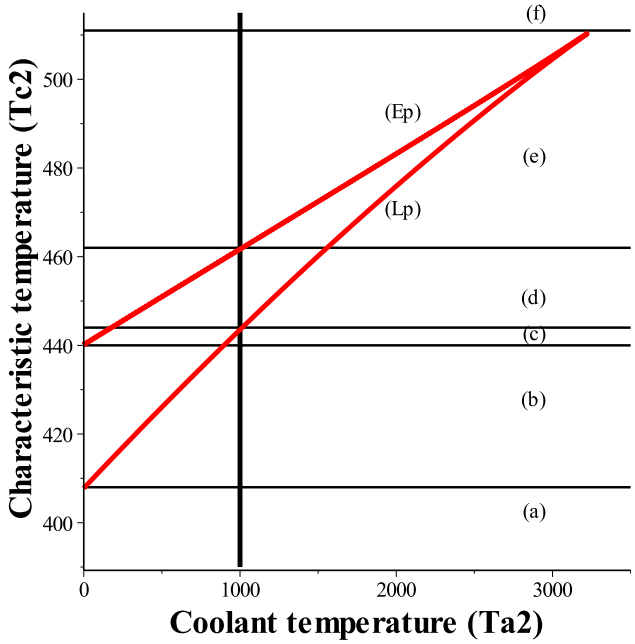

that the reaction takes place in a reactor cascade in which catalysts for the first and second reactions are placed in the first and second reactors, respectively. As there is no recycling, the steady-state behaviour in the first reactor is independent of that in the second reactor. We first examined the operating conditions required in the first reactor to obtain a minimum of 90% conversion. Realistic feed temperatures require high activation energy, high coolant temperature, low characteristic temperature and low endothermicity in the first reactor to achieve specified conversion. Thereafter, we fixed the catalyst in the first reactor and examined how the choice of the catalyst and

Table 3: The default parameter values are taken from [3], [7, pp. 110] and [10].

parameter	value
S_1	$23.22576\,\mathrm{m}^2$
S_2	$23.22576\,\mathrm{m}^2$
V_1	$1.35936\,\mathrm{m}^3$
V_2	$1.35936\,\mathrm{m}^3$
A_0	$8008.298025\,\mathrm{mol\,m}^{-3}$
T_0	$403\,\mathrm{K}$
R	$8.31441\,\mathrm{J\,K}^{-1}\mathrm{mol}^{-1}$
c_{pg}	$3.140\,\mathrm{J\,mol}^{-1}\mathrm{K}^{-1}$
ρ	$801.554 \times 10^3\,\mathrm{mol\,m}^{-3}$
χ_1	$851.735\,\mathrm{J\,s}^{-1}\mathrm{m}^{-2}\mathrm{K}^{-1}$
χ_2	$851.735\,\mathrm{J\,s}^{-1}\mathrm{m}^{-2}\mathrm{K}^{-1}$
α	$20/60\,\mathrm{K\,s}^{-1}$

coolant temperature in the second reactor effected the product concentration leaving the reactor. We found that there are six steady-state diagrams for the chosen parameters. The best possible catalysts, which produce autothermal behavior, have the ignition limit point occurring at an unphysical value (negative!) of the coolant temperature.

Acknowledgements MS is grateful to the Libyan government for a PhD scholarship. The authors thank the referee for their careful reading of our manuscript. The authors also thank Dr. J. E. Bunder for detailed commentary on our article.

A Nomenclature

Tables 3 and 4 give all parameter values.

Table 4: These physical parameters are chosen for illustration.

parameter	value
E_1	$50 \times 10^3\,\mathrm{J\,mol^{-1}} \leqslant E_1 \leqslant 180 \times 10^3\,\mathrm{J\,mol^{-1}}$
E_2	$50 \times 10^3\,\mathrm{J\,mol^{-1}}$
Q_1	$50 \times 10^3\,\mathrm{J\,mol^{-1}} \leqslant E_1 \leqslant 180 \times 10^3\,\mathrm{J\,mol^{-1}}$
Q_2	$100 \times 10^3\,\mathrm{J\,mol^{-1}}$
T_{c1}	$342\,\mathrm{K} \leqslant T_{c1} \leqslant 942\,\mathrm{K}$
T_{c2}	$342\,\mathrm{K} \leqslant T_{c2} \leqslant 942\,\mathrm{K}$
$T_{a,1}$	$300\,\mathrm{K} \leqslant T_{a,1} \leqslant 1000\,\mathrm{K}$
$T_{a,2}$	$300\,\mathrm{K} \leqslant T_{a,2} \leqslant 1000\,\mathrm{K}$
τ_1	$8\,\mathrm{s}$
τ_2	$8\,\mathrm{s}$

References

[1] O. Bilous and N. R. Amundson. Chemical reactor stability and sensitivity. *AIChE J.* 1(4):513–521, 1955. doi:10.1002/aic.690010422. C117

[2] G. Dangelmayr and I. Stewart. Sequential bifurcations in continuous stirred tank chemical reactors coupled in series. *SIAM J. Appl. Math.* 45(6):895–918, 1985. doi:10.1137/0145054. C105

[3] N. Devia and W. L. Luyben. Reactors: size versus stability. *Hydrocarbon Process.* 57(6):119–122, 1978. https://www.researchgate.net/publication/280895391_Reactors_Size_versus_Stability C121

[4] L. F. Razon and R. A. Schmitz. Multiplicities and instabilities in chemically reacting systems — a review. *Chem. Eng. Sci.* 42(5):1005–1047, 1987. doi:10.1016/0009-2509(87)80055-6. C115

[5] P. Gray and S. K. Scott. *Chemical Oscillations and Instabilities: Non-linear Chemical Kinetics.* Oxford University Press, 1990.

https://global.oup.com/academic/product/chemical-oscillations-and-instabilities-9780198558644?cc=au&lang=en& C105, C115

[6] G. Kolios, J. Frauhammer, and G. Eigenberger. Efficient reactor concepts for coupling of endothermic and exothermic reactions. *Chem. Eng. Sci.* 57:1505–1510, 2002. doi:10.1016/S0009-2509(02)00022-2. C103

[7] W. L. Luyben. *Processing Modelling, Simulation and Control for Chemical Engineering.* http://dl.acm.org/citation.cfm?id=542227 McGraw-Hill, New York, 1973. C121

[8] B. Lindstrom, J. A. J. Karlsson, P. Ekdunge, L. De Verdier, B. Haggendal, J. Dawody, M. Nilsson, and L. J. Pettersson. Diesel fuel reformer for automotive fuel cell applications. *Int. J. Hydrogen Energ.* 34:3367–3381, 2009. doi:10.1016/j.ijhydene.2009.02.013. C103

[9] L. Ma, C. Jiang, A. A. Adesina, D. L. Trimm, and M. S. Wainwright. Simulation studies of autothermal reactor system for H_2 production from methanol steam reforming. *Chem. Eng. J.* 62:103–111, 1996. doi:10.1016/0923-0467(95)03058-1. C103

[10] M. Nelson, G. Wake, and X. Chen. Heterogeneously catalysed combustion in a continuously stirred tank reactor— low-temperature reactions. *Combust. Theor. and Model.* 4(1):1–27, 2000. doi:10.1088/1364-7830/4/1/301. C105, C121

[11] K. Opoku-Gyamfi and A. A. Adesina. Kinetic studies of CH_4 oxidation over Pt-NiO/δ-Al_2O_3 in a fluidised bed reactor. *Appl. Catal. A: Gen.*, 180:113–122, 1999. doi:10.1016/S0926-860X(98)00340-8. C103

Author addresses

1. **M. M. Saleh**, School of Mathematics and Applied Statistics University of Wollongong, Wollongong, NSW 2522, Australia

mailto:mms907@uowmail.edu.au

2. **M. I. Nelson**, School of Mathematics and Applied Statistics University of Wollongong, Wollongong, NSW 2522, Australia
mailto:nelsonm@member.ams.org